Multifunctional Coumarin-Derived Metal Complexes: Synthesis, Bio-Screening, and *In Silico* Target Evaluation

Zulfiqar Ali Shahid and Rukhsana Tabassum*

Institute of Chemistry, The Islamia University of Bahawalpur, Hasilpur Road, Bahawalpur 63100, Pakistan

* ***Corresponding author:***

email: rukhsana.tabassum@iub.edu.pk

Received: August 14, 2025
Accepted: October 5, 2025

DOI: 10.22146/ijc.110413

Abstract: *Antibiotic resistance and oxidative stress-related diseases are emerging as serious global health concerns. These challenges underscore the urgent need for novel, effective, and environmentally friendly therapeutic agents. Coumarin derivative (ZL) and its Mn(II) and Zn(II) metal complexes were synthesized. Structural characterization was performed using various analytical techniques, including FTIR, XRD, ^{1}H-NMR, ^{13}C-NMR, TGA, and MS. FTIR spectra confirmed the existence of the –N=N– functional group of the coumarin-derived ligand. The antioxidant potential of the coumarin-derived compounds (against DPPH and NO) was evaluated. The ZL exhibited the most potent activity, with IC_{50} values of 6.48 μg/mL for the DPPH assay and 6.91 μg/mL for the NO radical scavenging assay. Antibacterial activities were evaluated against both Gram-negative and Gram-positive bacteria. Molecular docking studies further supported the biological potential of Zn-ZL, which showed strong binding affinities to oligo-1,6-glucosidase (PDB ID: 3AJ7) and mannosyl-oligosaccharide glucosidase (PDB ID: 4J5T), with binding energies of −8.5 and −9.4 kcal/mol, respectively. These findings revealed the therapeutic potential of coumarin-derived compounds and their metal complexes, particularly in addressing oxidative stress and antibiotic resistance.*

Keywords: *coumarin derivatives; metal complexes; antioxidant activity; antibacterial activity; molecular docking*

■ INTRODUCTION

The coumarin was isolated in 1820 by Vogel [1]. Coumarins are known for their characteristic sweet fragrance (vanilla-like); they appear as white crystalline powders with a pleasant, nutty-aromatic odor [2]. Coumarins are gaining significant attention in medicinal chemistry due to their broad spectrum of physiological and pharmacological activities [3]. These heterocyclic organic compounds, which contain a benzopyrone ring system, serve as effective electron donors and possess significant potential in metal-based drug development, particularly in the treatment of sensitive cancers [4]. The structural features of coumarins lead to versatile applications in analytical, biological, and synthetic fields [5].

Coumarins have antimicrobial and antioxidant activities [6]. Metal complexes of coumarins exhibit medicinal applications and display greater biological activity compared to their ligands [7]. It is worth mentioning that the chelating ability of coumarin derivatives enhances their biological activity [8]. Additionally, synthetic coumarins have found applications as fluorescent brightening agents, in the textile, detergent, paper, and dye industries [9]. Recent studies are based on the synthesis and biological evaluation of bivalent metal complexes [10]. Schiff bases are well known for their versatile coordination modes and biological relevance. These ligands form biologically active metal complexes, especially hydroxy-substituted coumarins, which exhibit strong antioxidant and metal-chelating properties [11]. The antioxidant activity of metal complexes is influenced by both the metal and the ligands.

Coumarin-based heterocycles play a vital role in medicinal and pharmaceutical applications. Understanding the synthesis of their biological activities is crucial for understanding their potential in drug

development and disease treatment [12]. The objective of this study was to synthesize coumarin-derived Mn(II) and Zn(II) complexes and evaluate their biological potential. The structural characteristics of the synthesized ligand and metal complexes were determined through ^{1}H-NMR, ^{13}C-NMR, FTIR, XRD, TGA, and MS, which are used to infer the structure and different thermodynamic activation parameters.

■ EXPERIMENTAL SECTION

Materials

Chemicals used during this study are 4-hydroxycoumarin, 3-aminophenol, 3-aminobenzoic acid, sodium nitrite ($NaNO_2$), HCl, NaOH, and solvents such as ethanol, methanol, distilled water, dimethyl sulfoxide, carbon tetrachloride, tetrahydrofuran, acetone, benzene, *n*-hexane, chloroform, and dimethylformamide (DMF) were purchased from Sigma-Aldrich, Merck, Alfa Aesar, and BDH, and were used without further purification.

Instrumentation

Silica gel plates were used to monitor the reaction progress by thin-layer chromatography, which was visualized under UV light. Melting points were recorded using the open capillary method on a Stuart SMP10 and are uncorrected. The FTIR spectra were obtained using a BRUKER Tensor 27 (M15E-PS/09) FTIR spectrophotometer, using KBr discs. The spectral range was covered from 4000 to 400 cm^{-1}. The ^{13}C- and ^{1}H-NMR spectra were acquired using a Bruker-300 MHz spectrometer. The DPPH and NO scavenging activities were assessed using an Optima SP300 Spectrophotometer. UV-vis spectra were recorded using an ELISA reader. Powdered XRD data were obtained using a BRUKER D8 X-ray diffractometer. The molecular mass of the compounds was measured using a JEOL 600H-1 mass spectrometer. TGA analysis was recorded on a Shimadzu TGA-50H.

Procedure

Synthesis of coumarin derivative

The synthesis of the coumarin-based azo ligand ZL is illustrated in Scheme 1 and briefly described as follows: a 10 mL aqueous solution of 3 M HCl was prepared and added to 4-aminophenol (a), creating an acidic medium suitable for diazotization. Then, an aqueous solution of $NaNO_2$ was added dropwise at 0–5 °C under continuous stirring for 20 min, forming the corresponding diazonium salt (b) [13]. In a separate step, 4-hydroxycoumarin (c) was dissolved in an alkaline medium. The freshly prepared

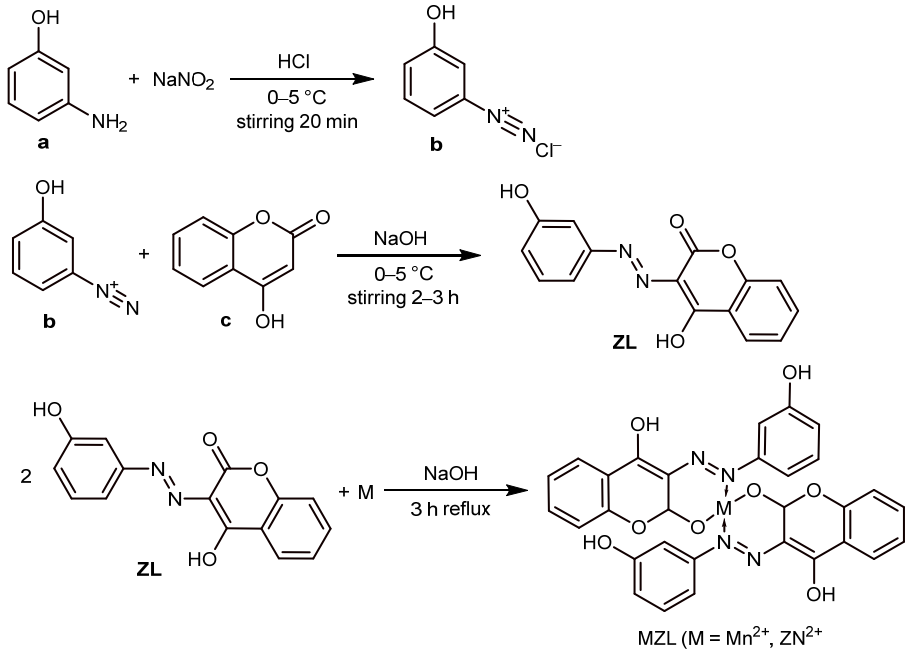

Scheme 1. Synthesis scheme of ZL and its metal complexes

diazonium salt solution was added slowly to this cold alkaline solution, and the azo coupling reaction was allowed to proceed at 0–5 °C for 2–3 h, resulting in the formation of the azo-linked coumarin ligand (ZL) [14]. After coupling, the pH of the reaction mixture was adjusted using a 3 M NaOH, and the solution was refluxed for 3 h to ensure completion. The reaction mixture was then cooled, and the product was washed with cold distilled water and purified by recrystallization using diethyl ether [15]. The final ligand ZL was obtained with a yield of up to 87%. The reaction progress and completion were monitored using TLC.

Metallization of ligand ZL

For the synthesis of Mn^{2+} and Zn^{2+} metal complexes, a solution of 0.125 g (0.5 mmol) of the coumarin derivative was prepared in 10 mL of ethanol and stirred continuously for 5 min. Subsequently, an ethanolic solution of the metal salts (Zn^{2+} or Mn^{2+}) was added in a 1:2 metal-to-ligand ratio, and the mixture was stirred for 20 min [16]. NaOH was then added dropwise under reflux conditions to adjust the pH to approximately 8, ensuring a basic medium. A visible color change was observed, indicating the formation of the metal complex (M-ZL). The reaction was allowed to proceed under reflux for 2 h. The product was collected, washed with distilled water, and dried for further use [10].

Free radical scavenging assays

The antioxidant activities of ZL, Mn-ZL, and Zn-ZL were evaluated using 2,2-diphenyl-1-picrylhydrazyl (DPPH) and nitric oxide (NO) free radical scavenging. For the DPPH assay, various concentrations (i.e., 5–25 µg/mL) of the test compounds were prepared, with ascorbic acid serving as the standard. Absorbance was recorded at 517 nm [17]. For the NO scavenging assay, nitric oxide was produced via sodium nitroprusside at pH 7.4 in phosphate-buffered saline. A 2 mL of each sample solution (5–25 µg/mL in DMSO) was mixed with 2.5 mL of 8 mM sodium nitroprusside in PBS. The mixture was incubated at 25 °C for 4 h. Then, 2 mL of Griess reagent and 1 mL of 0.1% *N*-(1-naphthyl)ethylenediamine dihydrochloride were added, followed by incubation at 25 °C for 30 min. After that, the absorbance of the mixture was measured at 546 nm. A solution with DMSO instead of the test compound was used as a blank. All experiments were conducted in triplicate, and %scavenging activity was calculated using Eq. (1) [18].

$$\%\text{Scavenging} = \frac{(A_0 - A_s)}{A_0} \times 100\% \quad (1)$$

Antibacterial activities

The ZL, Mn-ZL, and Zn-ZL compounds were investigated for their antibacterial activity against various bacteria. The zone of inhibition by ZL, Mn-ZL, and Zn-ZL was measured using the disc diffusion method against a 24 h culture of selected bacteria [19]. The gram-negative bacteria *Eschericia coli* and *Pseudomonas aeruginosa* were used, while the gram-positive bacteria were *Staphylococcus Pyogenes* and *Bacillus.* Amikacin was used as a standard drug for evaluating antibacterial activity [20].

Molecular docking

The binding interactions of ZL, Mn-ZL, and Zn-ZL with two enzymes, namely mannosyl-oligosaccharide glucosidase and oligo-1,6-glucosidase, were evaluated. For this purpose, 3D crystal structures of these enzymes were obtained from the Protein Data Bank. Before conducting the docking analysis, the target protein structures were prepared using MGLTools. Heteroatoms and H_2O were removed from protein structures. Additionally, polar hydrogen atoms and Kollman controls were added to ensure the accurate representation of the protein structures. The 3D structures of the synthesized ZL were drawn using ChemDraw 3D. These structures were then subjected to energy minimization to obtain their most stable conformations. AutoDock was employed in its default genetic algorithm as the scoring function. The compounds were docked into the active pockets of mannosyl-oligosaccharide glucosidase and oligo-1,6-glucosidase enzymes. The center of the grid box was set as x: 21.306612, y: −0.461484, z: 18.843785 for mannosyl-oligosaccharide glucosidase and x: −18.523631, y: −20.732132, z: 8.202425 for oligo-1,6-glucosidase to define the search space for docking, respectively. Multiple docking configurations were generated for each compound and enzyme, resulting in approximately

100 different configurations. Finally, to gain deeper insight into the binding interactions within the active sites of mannosyl-oligosaccharide glucosidase and oligo-1,6-glucosidase, the most stable configurations were selected for further analysis. Subsequently, 2D and 3D interaction models were developed to improve understanding of the binding behavior of the derivatives within these enzyme active sites [21].

Chemistry

Coumarin derivative ZL and its metal complexes with Mn^{2+} and Zn^{2+} were synthesized (Scheme 1) and subjected to characterization to evaluate their physical and structural properties. These included solubility, melting point, and various spectroscopic techniques such as XRD, UV–vis, FTIR, and TGA. Job's method was employed to determine the optimal stoichiometric ratio, and it was observed that a 2:1 ratio of ligands to metals yielded the highest absorbance [22]. Consequently, the metal complexes were synthesized utilizing this specific stoichiometric ratio of ligands and metal salts [23]. Regarding the thermal stability of these metal complexes, it was observed that the Mn(II) and Zn(II) complexes exhibited melting points between 200 and 300 °C, while the coumarin derivatives themselves displayed a melting point range of 150 to 400 °C. This discrepancy indicates that the metal coordination compounds of the derivatives exhibit enhanced stability due to the smaller size and higher charge of the Mn and Zn complexes [24]. Furthermore, complexes demonstrated solubility in DMSO.

Characterization

4-Hydroxy-3-[(*E*)-(3-hydroxyphenyl)diazenyl]-2*H*-chromen-2-one (ZL). Dark Brown solid, Yield: 70.90%, Rf: 0.71 (acetone:CCl_4 (7:3)), m.p.: 210 °C, soluble in acetone, ethanol, methanol, DMSO, THF, DMF and *n*-hexane, FTIR (KBr disc, cm^{-1}): 3354 (NH stretch, O–H str.), 2887 (C–H str.), 1600 (N=N str.), 1547 (C=C str.), 1330 (C–C str.), 1284 (C–N str.), 1143 (C–O str.), UV-vis λ_{max} (DMSO, nm): 620, ^{1}H-NMR (300 MHz, $CDCl_3$-D) δ 12.51 (*s*, OH), 7.81 (*dd*, *J* = 7.9, 1.4 Hz, Hf), 7.65–7.61 (*m*, He, Hh), 7.37–7.32 (*m*, Hg, a-d). ^{13}C-NMR (100 MHz, DMSO) δ 165.6 (C4), 162.9 (C9), 160.4 (C16), 158.7 (C6), 150.0 (C10), 145.2 (C18), 142.7 (C5, C3, C9), 141.9 (C14), 136.3 (C19), 132.8 (C7), 132.1 (C17), 130.8 (C15), 123.1 (C8). EI-MS *m/z*: Required for $C_{15}H_{10}N_2O_4^{+\bullet}$: 282.25 found 282.20.

4-Hydroxy-3-[(*E*)-(3-hydroxyphenyl)diazenyl]-2*H*-chromen-2-one manganese complex (Mn-ZL). Light pink solid, m.p.: 210 °C, Yield: 77.33%, soluble in acetone, DMSO, benzene, CCl_4, ethanol, methanol, chloroform, THF, DMF and *n*-hexane, FTIR (KBr disc, cm^{-1}): 3352 (NH, O–H str.), 2879 (C–H str.), 1642 (C=O str.), 1596 (N=N stretch), 1551 (C=C str.), 1322 (C–C str.), 1240 (C–N str.), 1198 (C–O str.), 758 (Mn–O), 620 (Mn–N), UV-vis λ_{max} (DMSO, nm): 660.

4-hydroxy-3-[(*E*)-(3-hydroxyphenyl)diazenyl]-2*H*-chromen-2-one zinc complex (Zn-ZL). Light brown solid, m.p.: > 300 °C, Yield: 72.90%, soluble in acetone, DMSO, benzene, CCl_4, ethanol, methanol, chloroform, THF, DMF and *n*-hexane, FTIR (KBr disc, cm^{-1}): 3361 (NH, O–H stretch), 2893 (C–H str.), 1642 (C=O str.), 1596 (N=N str.), 1550 (C=C str.), 1518 (C–C str.), 1196 (C–N str.), 952 (C–O str.), 736 (Zn–O), 577 (Zn–N), UV-vis λ_{max} (DMSO, nm): 660.

■ RESULTS AND DISCUSSION

FTIR

FTIR of synthesized compounds gave valuable information about the structure of synthesized compounds. The FTIR spectra showed prominent peaks of functional groups, such as O–H, C–H, C=O, C=N, N=N, C=C, C–N, and C–O, which confirm the formation of a ZL coumarin derivative [25]. The FTIR spectra of the ligands showed a broad O–H stretching band in the range of 3650–3200 cm^{-1} and an N–H stretching band around 3600–3400 cm^{-1}. The vibrational frequency for the C–H sp^2 stretch was observed around 3000–2800 cm^{-1}. A distinctive peak corresponding to the N=N stretching vibration of the diazenyl group emerged at 1700–1400 cm^{-1}. Due to the broad nature of the O–H stretching band, it overlapped with the aromatic C–H stretch in this region. A characteristic C=C stretching vibration appeared near 1520–1400 cm^{-1}, while the aromatic C–N stretch was observed between 1390–1180 cm^{-1}. The C–O stretching vibration was noted in the range of 1320–900 cm^{-1}. Upon coordination with Mn^{2+} and Zn^{2+}, the N=N, C=O,

and C–N vibrations shifted slightly, and shifts in these bands confirmed metal–ligand interactions [26]. The M–O stretches appeared below 700 cm^{-1}, confirming the successful complexation as given in Fig. 1(a).

TGA

The thermogravimetric analysis of ZL, ZL–Mn, and ZL–Zn was conducted, and the corresponding curves are shown in Fig. 1(b–d). Each compound exhibits multiple thermal degradation steps, reflecting differences in stability and decomposition pathways. For the ligand ZL (Fig. 1(b)), four decomposition stages were observed. The first stage (20–190 °C) corresponds to the loss of adsorbed moisture, with a mass loss of 1.52% [27]. The second stage (190–300 °C) is attributed to N_2 elimination, resulting in a 9.58% mass loss. The third stage (300–600 °C) accounts for a 14.25% loss, likely due to the evolution of CH_4 and further degradation of the organic framework [28]. The residual mass was identified as $C_9H_{17}O_2$; the DSC curve displays endothermic peaks at 301 °C corresponding to major structural breakdown steps. For the Mn(II) complex (Fig. 1(c)), the TGA curve shows three decomposition stages. The first stage (20–400 °C) involves a 3.97% mass loss, attributed to the release of water molecules. The second stage (400–600 °C) corresponds to the elimination of N_2, resulting in a 4.73% mass loss. The third stage (600–880 °C) results in a 9.72% loss, likely due to the release of C_2H_6. The final residue, $C_{29}H_{57}MnO_2$, suggests enhanced thermal stability compared to the free ligand [29]. The DSC curve reveals endothermic peaks at 602 °C. In the case of the Zn(II) complex (ZL–Zn, Fig. 1(d)), the decomposition

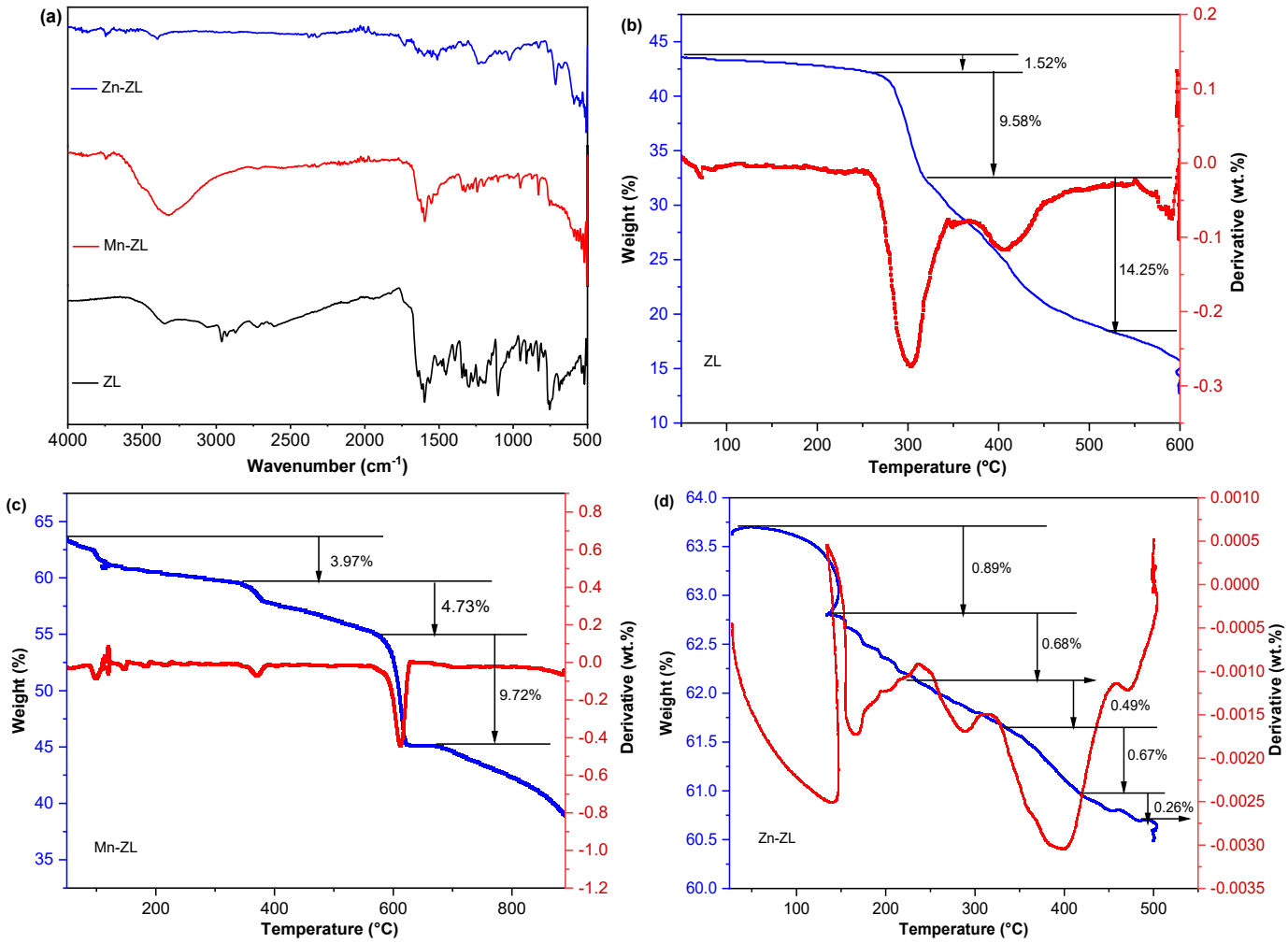

Fig 1. (a) FTIR spectra and TGA spectra of (b) ZL, (c) Mn-ZL, and (d) Zn-ZL

pattern is similar. The first stage (20–120 °C) shows a 0.89% mass loss corresponding to the release of H_2O. The second stage (120–300 °C) involves N_2 elimination with 0.68 + 0.49% loss, while the third stage (300–500 °C) shows a 0.67 + 0.26% loss, attributed to CH_4 evolution. Overall, the TGA results highlight distinct thermal behavior for each compound; however, metal complexes exhibit improved thermal stability as compared to ligand ZL [30].

^{1}H-NMR

^{1}H-NMR spectroscopy is an important analytical method for determining the structure of substances associated with the proton in the molecule of the analyzed product. In the ^{1}H-NMR spectrum of ZL (Fig. S1(a)), a sharp singlet at 15.25 ppm confirms the presence of exchangeable hydroxyl protons (–OH), likely from the phenolic group [31]. Another notable peak at 3.78 ppm also indicates the presence of a hydroxyl proton. Aldehyde protons typically resonate between 9.5 and 10.3 ppm, but in this case, no distinct aldehyde peak is present, suggesting its absence. Aromatic proton signals appear as multiple peaks between 7.36 and 8.28 ppm. Specifically, the proton labeled Hf resonates at 8.28 ppm, Hd at 7.88 and 7.78 ppm, He at 7.62 ppm, Hh at 7.40 ppm, and Ha, Hb, Hg at 7.36 ppm, consistent with the substituted aromatic structure [32]. This spectral data confirms the successful synthesis and structural integrity of the ZL ligand, as evidenced by well-resolved aromatic and phenolic proton signals.

^{13}C-NMR

The ^{13}C-NMR spectrum of the ZL compound (Fig. S1(b)) was recorded using a Bruker AM400 MHz spectrometer in DMSO-d_6. The observed chemical shifts confirm the successful synthesis of the coumarin-based azo derivative, highlighting distinct carbon environments within the molecule. A sharp signal at 165.6 ppm corresponds to C–OH groups, specifically C21 and C4 [33]. The carbon atoms C2 and C6, likely influenced by electron-withdrawing substituents, appear at 161.8 and 153.5 ppm, respectively. The aromatic region exhibits several peaks, with C18 and C15 resonating at 132.6 ppm, while C8, C14, and C19 are found at 123.9 ppm. Further downfield, C9, C7, and C5 appear at 116.3 ppm, and C10 at 115.7 ppm. A downfield shift at 90.9 ppm is attributed to C3, located within the conjugated ring system. Carbons associated with the azo linkage are observed in the 136–152 ppm range, consistent with the expected diazenyl structure [34]. These assignments collectively support the structure of the ZL compound and are in good agreement with literature values for coumarin-azo derivatives.

XRD

Powder XRD is a useful and informative technique for providing insight into the crystalline or amorphous nature of ligands and their metal complexes. Due to the very small crystal size of coumarin ligands and their complexes, single-crystal XRD data could not be obtained. However, powder XRD data were recorded to determine the structural information and crystalline pattern of the synthesized derivatives and their complexes. The XRD patterns of ZL, Mn–ZL and Zn–ZL are displayed in Fig. 2(a). The ligand ZL exhibits multiple sharp and intense peaks in the 2θ range of 10° to 60°, indicating its crystalline nature. In contrast, the XRD spectra of both Mn–ZL and Zn–ZL complexes show broad and less intense peaks, suggesting a significant reduction in crystallinity upon metal coordination [35]. The broad humps in the patterns of the metal complexes are characteristic of amorphous or poorly crystalline structures. The broadening of diffractions in the case of complexes confirms successful metal chelation and structural modification. The absence of sharp diffraction peaks in Mn–ZL and Zn–ZL supports the formation of new coordination compounds with altered crystal packing and reduced long-range order [36].

UV-vis Spectroscopy

The UV-vis spectra of ZL, Mn–ZL, and Zn–ZL were recorded in DMSO at room temperature using 50 ppm solutions over the wavelength range of 300–800 nm, as shown in Fig. 2(b). The free ligand ZL exhibited a strong absorption peak (λ_{max}) at 320 nm, which corresponds to the π–π^* electronic transition, along with a minor n–π^* transition at 500 nm [37]. Upon complexation with Mn(II) and Zn(II), noticeable bathochromic shifts were observed, and the complex shows λ_{max} at 660 nm. These results highlight the successful coordination of metal ions and the ligand [38].

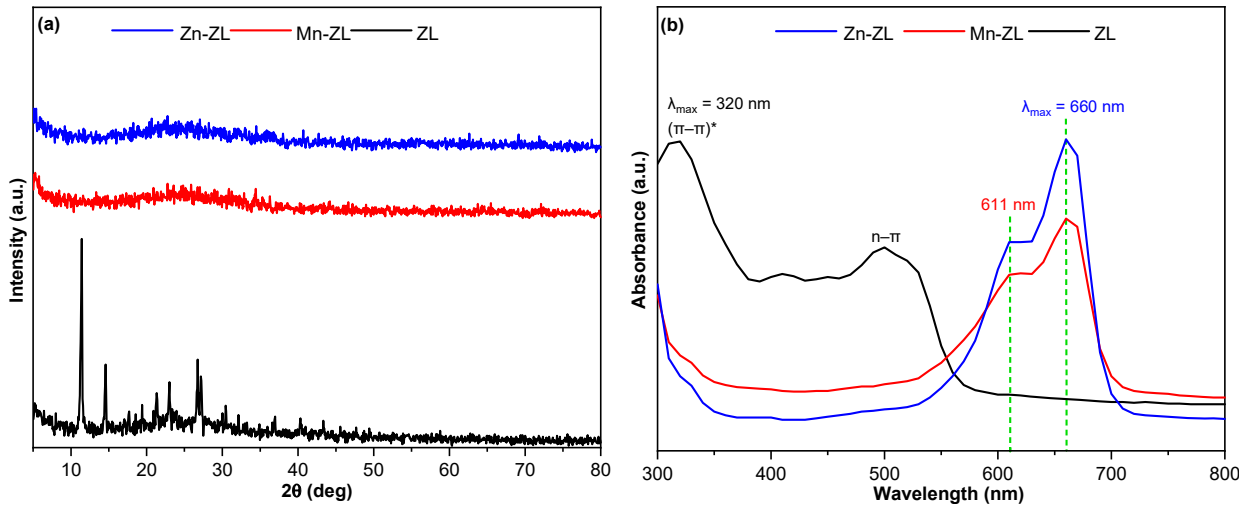

Fig 2. (a) XRD pattern, (b) UV-vis spectra of ZL, Mn–ZL, Zn–ZL

MS

Mass spectrometry provides not only the mass-to-charge ratio (*m/z*) of the intact molecular ion, but also detailed information about its fragmentation pathways. By analyzing these fragmentation patterns, it is possible to deduce the unique structural characteristics of a compound. It is also fundamental for assessing the purity and identity of a synthesized substance. The molecular mass of the ZL ligand is 310.2, which was confirmed by the molecular ion peak in Fig. S2. However, this is not the most intense peak. In contrast to the molecular ion, the base peak (most intense) for this ligand appears at *m/z* 120.0. Another prominent peak is observed at *m/z* 162.0. The possible modes of fragmentation for the ZL ligand are shown in Fig. S3. An important fragmentation route begins with the loss of a carbon monoxide group from a fragment with *m/z* 310.2, leading to a new fragment ion at *m/z* 282.25 [39]. Furthermore, this ion yields a significant peak at *m/z* 162.02. This pathway is followed by the loss of a neutral molecule from the *m/z* 162.02 ion, resulting in a fragment at *m/z* 92.03. A second major fragmentation pathway leads to a prominent peak at *m/z* 120.0. The fragmentation of this ion involves the loss of a carbon dioxide group, which gives rise to a fragment at *m/z* 77.03. Subsequent fragmentation of the *m/z* 77.03 ion yields a fragment at *m/z* 43.0.

Free Radical Scavenging

The scavenging potential of DPPH is a simple, efficient, and relatively stable free radical method in which hydrogen or an electron is accepted by the reduction of the free radical with the help of an antioxidant molecule. The DPPH radical solution has a purple color. When an antioxidant is added, it reduces the DPPH radical, causing its color to change to yellow. The greater the color change, the more DPPH radicals have been scavenged, indicating enhanced antioxidant activity [40]. The activity of ZL, Mn–ZL, and Zn–ZL was evaluated at five different concentrations (5–25 µg/mL). Ascorbic acid was used as the standard reference, as shown in Table 1 and Fig. 3(a–c). The calculations were based on the absorbance at 579 nm, and the results of the antioxidant potential of the prepared compounds are expressed as the

Table 1. IC_{50} values of Scavenging of DPPH and NO assay of ZL and their metal complexes

Compound	Scavenging of DPPH IC_{50} (µg/mL)	Scavenging of NO IC_{50} (µg/mL)
ZL	6.48 ± 0.03	6.91 ± 0.094
Mn-ZL	6.84 ± 0.05	6.27 ± 0.008
Zn-ZL	6.88 ± 0.05	6.46 ± 0.016
*AA	7.06 ± 0.04	6.79 ± 0.026

*AA=Ascorbic acid (standard compound)

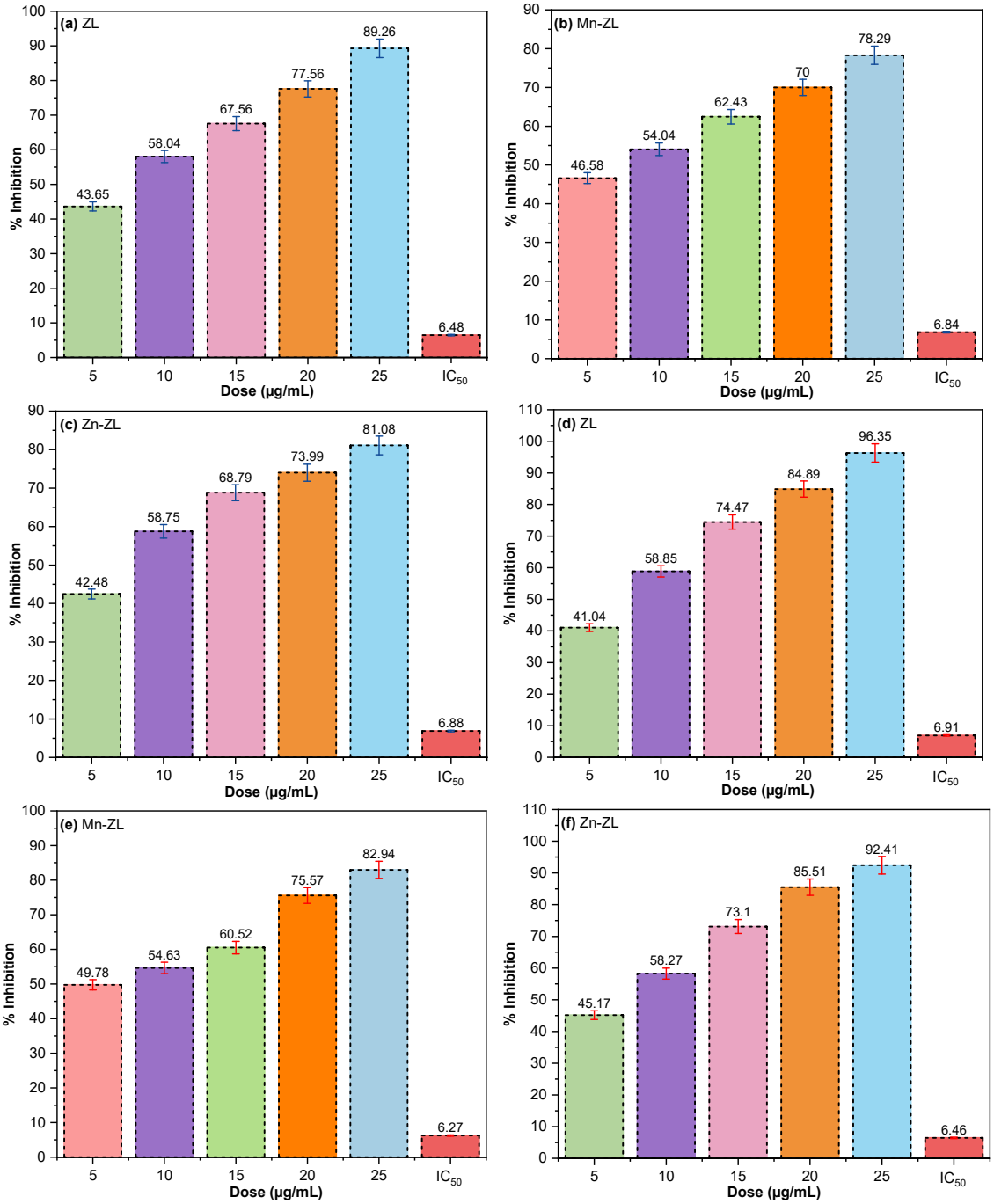

Fig 3. Comparative DPPH scavenging activity by (a) ZL compounds, (b) Mn–ZL, (c) Zn–ZL. Comparative NO scavenging activity by (d) ZL, (e) Mn–ZL, and (f) Zn–ZL

IC_{50} value. All the prepared compounds display good to moderate inhibition potential as compared to the standard (7.06 µg/mL).

NO is a free radical with dual roles: it is essential for various biological functions, but also contributes to oxidative damage. The study evaluated the ability of synthesized coumarin ligands and their metal complexes to scavenge nitric oxide. This was done by measuring the inhibition of nitrite ions at 546 nm using the Griess reagent. The results showed that synthesized compounds are more effective at scavenging nitric oxide. The NO radical scavenging activity of five concentrations (5–

25 µg/mL) of ZL, Mn–ZL, and Zn–ZL compared with ascorbic acid (AA = 7.06 µg/mL), and the results are shown in Fig. 3(d–f). The results of the antioxidant potential of the prepared compounds are expressed as IC_{50} values. All the prepared compounds display good to moderate inhibition potential as compared to the standard (ascorbic acid) [41].

Antibacterial Activity

The antibacterial efficacy of the synthesized compounds ZL, Mn–ZL, and Zn–ZL was evaluated against *E. coli*, *Pseudomonas*, *S. pyogenes*, and *Bacillus*. The results are illustrated in Fig. S4, and their findings are tabulated in Table 2. The results reveal that the Zn–ZL complex exhibits superior antibacterial activity as compared to ZL, Mn–ZL, and Amikacin. The Zn–ZL shows 13, 19, 15, and 18 mm against *E. coli*, *Pseudomonas*, *S. pyogenes*, and *Bacillus*, respectively. This enhanced activity is attributed to the interaction of metal ions with nitrogen. These results suggest that the synthesized zinc complex holds promise as a potent antimicrobial agent due to factors such as free electron mobility and the availability of coordinating sites.

Molecular Docking Analysis

To understand the mechanism of the antidiabetic potential, the molecular interaction between the synthesized ligands and two specific enzymes, oligo-1,6-glucosidase (PDB ID: 3AJ7) and mannosyl-oligosaccharide glucosidase (PDB ID: 4J5T), was investigated. The resolution of the oligo-1,6-glucosidase structure was 1.30 Å, while the resolution of the mannosyl-oligosaccharide glucosidase structure was 2.04 Å. The study's results revealed that hydrogen bonds formed when a hydrogen atom interacted with an electronegative atom, such as oxygen or nitrogen. To investigate the binding interactions between the ZL and their metal complexes with the binding pocket of Mannosyl-oligosaccharide and Oligo-1,6-glucosidase, molecular docking analysis was conducted [42]. The docking analysis yielded compelling results, indicating strong binding interactions between several amino acid residues within the binding pockets of mannosyl-oligosaccharide glucosidase and oligo-1,6-glucosidase. The results are tabulated in Table 3.

Table 2. Antibacterial activity of ZL, Mn–ZL, and Zn–ZL

Compound	Zone of inhibition (mm)			
	Gram-negative bacteria		Gram-positive bacteria	
	E. coli	*Pseudomonas*	*S. pyogenes*	*Bacillus*
ZL	8	18	10	0
Mn-ZL	0	13	0	8
Zn-ZL	13	19	15	18
Amikacin	0	8	14	8

These findings provide valuable insights into potential lead compounds for drug development targeting mannosyl-oligosaccharide glucosidase and oligo-1,6-glucosidase. For 3AJ7, the ligands ZL, Mn–ZL, and Zn–ZL displayed binding energies of –8.7, –8.8, and –8.5 kcal/mol, respectively (Fig. S5). For 4J5T, ligands ZL, Mn–ZL, and Zn–ZL showed strong docking scores with binding energies of –9.4, –9.0, and –9.4 kcal/mol, respectively (Fig. S6).

■ CONCLUSION

In this research work, 4-hydroxy coumarin derivatives have been synthesized in high yields under mild reaction conditions, demonstrating both cost-effectiveness and atom economy. Structural characterization of the synthesized ligand and its metal

Table 3. Molecular docking of ZL with their metal complexes against mannosyl-oligosaccharide glucosidase and oligo-1,6-glucosidase

Compounds	PDB ID	Binding energy (kcal/mol)	Hydrogen bond interactions	Hydrophobic interactions
ZL	3AJ7	–8.7	-	Lys156, Tyr158, Arg315
Mn-ZL	3AJ7	–8.8	Lys523	Phe321, Leu323, Trp326, Phe360
Zn-ZL	3AJ7	–8.5	His280	Asp307, Pro312
ZL	4J5T	–9.4	Arg799	Glu402, Glu463, Arg727, Ile734, His803
Mn-ZL	4J5T	–9.0	Arg799	Phe7, Lys98, Arg304
Zn-ZL	4J5T	–9.4	Arg304, Met493	Phe7, Lys98

complexes confirmed the successful synthesis of new diazenyl compounds. The antioxidant screening revealed IC_{50} values of 6.48–6.88 and 6.27–6.97 µg/mL for the DPPH and NO assays. Antibacterial activity was assessed against Gram-negative bacteria (*E. coli* and *Pseudomonas*) and Gram-positive bacteria (*Staphylococcus pyogenes* and *Bacillus*), with inhibition zones ranging from 8 to 19 mm. Molecular docking studies indicated that Zn–ZL and Mn–ZL had excellent docking scores with binding energies of –9.0 and –9.4 kcal/mol, respectively. Overall, these findings promise the potential of the synthesized coumarin derivatives for various biological applications.

■ ACKNOWLEDGMENTS

The authors are grateful to the Institute of Chemistry-IUB for providing essential facilities. The authors also acknowledge the Higher Education Commission for providing the analysis facility via ASIP.

■ CONFLICT OF INTEREST

There are no financial or personal competing interests among the authors.

■ AUTHOR CONTRIBUTIONS

Zulfiqar Ali Shahid: Writing – original draft, Methodology, Investigation, Visualization. Rukhsana Tabassum: Writing – review & editing, Supervision, Project administration, Funding acquisition. All authors read and agreed to the final version of this manuscript.

■ REFERENCES

[1] Abd El-Nasser, M.G., and Abdel-Latif, S.A., 2023, Ligational behavior of bidentate nitrogen–oxygen donor 8-quinolinolazodye toward Ni^{2+} and Zn^{2+} ions: Preparation, spectral, thermal, experimental, theoretical, and docking studies, *Appl. Organomet. Chem.*, 37 (3), e6998.

[2] Abdi, G.F., and Tesfa, K.H., 2022, Recent advances in synthesis of coumarins: Coumarin derivatives and their biological application, *Ethiop. J. Nat. Comput. Sci.*, 2 (2), 361–374.

[3] Abdulraheem, S.S., and Hadi, M.K., 2021, Synthesis and characterization of new coumarin derivatives as possible antimicrobial agents, *Int. J. Drug Delivery Technol.*, 11 (4), 1484–1490.

[4] Abid, M.Z., Rafiq, K., Rauf, A., and Hussain, E., 2024, Unveiling the potential of MXene-fabricated catalysts: An effective approach for H_2 generation from water splitting, *Nanoscale Adv.*, 6 (23), 5861–5873.

[5] Dhiman, N., Kaur, K., and Jaitak, V., 2020, Tetrazoles as anticancer agents: A review on synthetic strategies, mechanism of action and SAR studies, *Bioorg. Med. Chem.*, 28 (15), 115599.

[6] Al-Majedy, Y., Al-Amiery, A., Kadhum, A.A., and BakarMohamad, A., 2017, Antioxidant activity of coumarins, *Syst. Rev. Pharm.*, 8 (1), 24–30.

[7] Al-Farraj, E.S., Alharbi, S.K., Feizi-Dehnayebi, M., Asghar, B.H., Alahmadi, N., Eskander, T.N.A., Alghamdi, M.A., and Abu-Dief, A.M., 2025, Molecular, stoichiometric, stability and biological investigations of novel multifunctional salen metal chelates: From synthesis to therapeutic potential supported by theoretical approaches, *Appl. Organomet. Chem.*, 39 (8), e70273.

[8] Banerjee, S., and Bhargava, B., 2024, Effect of electronegative atoms on π–π stacking and hydrogen bonding behavior in simple aromatic molecules—An Ab initio MD study, *J. Mol. Graphics Modell.*, 127, 108693.

[9] Bazargani, M.M., and Rohloff, J., 2016, Antibiofilm activity of essential oils and plant extracts against *Staphylococcus aureus* and *Escherichia coli* biofilms, *Food Control*, 61, 156–164.

[10] Benkhaya, S., M'rabet, S., and El Harfi, A., 2020, Classifications, properties, recent synthesis and applications of azo dyes, *Heliyon*, 6 (1), e03271.

[11] Bhate, P.M., Devi, R.V., Dugane, R., Hande, P.R., Shaikh, L., Vaidya, S., and Masand, S., 2017, A novel reactive dye system based on diazonium salts, *Dyes Pigm.*, 145, 208–215.

[12] Catapano, M.C., Karlíčková, J., Tvrdý, V., Sharma, S., Prasad, A.K., Saso, L., Chhillar, A.K., Kuneš, J., Pour, M., Parmar, V.S., and Mladěnka, P., 2018, Mono and dihydroxy coumarin derivatives: Copper chelation

and reduction ability, *J. Trace Elem. Med. Biol.*, 46, 88–95.

[13] Mamta, M., Subhash, S., Pinki, P., and Chaudhary, A., 2023, *In vitro* cytotoxicity and antimicrobial evaluation of novel 24–28 membered Schiff base octaazamacrocyclic complexes of manganese (II): Synthesis, characterization, DFT and molecular docking studies, *J. Mol. Struct.*, 1275, 134667.

[14] Conneely, A., McClean, S., Smyth, W., and McMullan, G., 2001, Study of the mass spectrometric behaviour of phthalocyanine and azo dyes using electrospray ionisation and matrix-assisted laser desorption/ionisation, *Rapid Commun. Mass Spectrom.*, 15 (22), 2076–2084.

[15] Dai, F., Zhuang, Q., Huang, G., Deng, H., and Zhang, X., 2023, Infrared spectrum characteristics and quantification of OH groups in coal, *ACS Omega*, 8 (19), 17064–17076.

[16] Das, R.K., Sharma, D., Paul, S., and Sengupta, D., 2023, Microwave-assisted synthesis of 3-amino-2-phenylquinazolin-4(3*H*)-one (QH) and 4-oxo-2-phenylquinazoline-3(4*H*)-carbothioamide (QTh), *Curr. Microwave Chem.*, 10 (1), 53–59.

[17] Dippong, T., Levei, E.A., and Cadar, O., 2021, Formation, structure and magnetic properties of $MFe_2O_4@SiO_2$ (M= Co, Mn, Zn, Ni, Cu) nanocomposites, *Materials*, 14 (5), 1139.

[18] Abd El-Lateef, H.M., El-Dabea, T., Khalaf, M.M., and Abu-Dief, A.M., 2023, Recent overview of potent antioxidant activity of coordination compounds, *Antioxidants*, 12 (2), 213.

[19] Garg, S.S., Gupta, J., Sharma, S., and Sahu, D., 2020, An insight into the therapeutic applications of coumarin compounds and their mechanisms of action, *Eur. J. Pharm. Sci.*, 152, 105424.

[20] Ghanghas, P., Choudhary, A., Kumar, D., and Poonia, K., 2021, Coordination metal complexes with Schiff bases: Useful pharmacophores with comprehensive biological applications, *Inorg. Chem. Commun.*, 130, 108710.

[21] Gonçalves Nunes, W.D., Mannochio Russo, H., da Silva Bolzani, V., and Caires, F.J., 2021, Thermal characterization and compounds identification of commercial *Stevia rebaudiana* Bertoni sweeteners and thermal degradation products at high temperatures by TG–DSC, IR and LC–MS/MS, *J. Therm. Anal. Calorim.*, 146 (3), 1149–1155.

[22] Gupta, A., Mumtaz, S., Li, C.H., Hussain, I., and Rotello, V.M., 2019, Combatting antibiotic-resistant bacteria using nanomaterials, *Chem. Soc. Rev.*, 48 (2), 415–427.

[23] Houas, N., Chafaa, S., Chafai, N., Ghedjati, S., Djenane, M., and Kitouni, S., 2022, Synthesis, characterization, DFT study and antioxidant activity of (2-hydroxynaphthalen-1-yl) methyl 2-hydroxyphenyl amino phosphonic acid, *J. Mol. Struct.*, 1247, 131322.

[24] Kaur, H., Lim, S.M., Ramasamy, K., Vasudevan, M., Shah, S.A.A., and Narasimhan, B., 2020, Diazenyl Schiff bases: Synthesis, spectral analysis, antimicrobial studies and cytotoxic activity on human colorectal carcinoma cell line (HCT-116), *Arabian J. Chem.*, 13 (1), 377–392.

[25] Mabrouk, M., Hammad, S.F., Abdelaziz, M.A., and Mansour, F.R., 2018, Ligand exchange method for determination of mole ratios of relatively weak metal complexes: A comparative study, *Chem. Cent. J.*, 12 (1), 143.

[26] Mikheev, Y.A., and Ershov, Y.A., 2018, Assignment of the $\pi\rightarrow\pi^*$ and $n\rightarrow\pi^*$ transitions to the spectral bands of azobenzene and dimethylaminoazobenzene, *Russ. J. Phys. Chem. A*, 92 (8), 1499–1507.

[27] Moreira, J.M., Campos, G.F., de Campos Pinto, L.M., Martins, G.R., Tirloni, B., Schwalm, C.S., and de Carvalho, C.T., 2022, Copper (II) complexes with novel Schiff-based ligands: Synthesis, crystal structure, thermal (TGA–DSC/FT-IR), spectroscopic (FT-IR, UV-Vis) and theoretical studies, *J. Therm. Anal. Calorim.*, 147 (6), 4087–4098.

[28] Mustafa, Y.F., Kasim, S.M., Al-Dabbagh, B.M., and Al-Shakarchi, W., 2023, Synthesis, characterization and biological evaluation of new azo-coumarinic derivatives, *Appl. Nanosci.*, 13 (2), 1095–1102.

[29] Ngamsurach, P., and Praipipat, P., 2022, Comparative antibacterial activities of *Garcinia cowa* and *Piper sarmentosum* extracts against *Staphylococcus*

aureus and *Escherichia coli* with studying on disc diffusion assay, material characterizations, and batch experiments, *Heliyon*, 8 (11), e11704.

[30] Padvi, K.S., Sarkate, A.P., Bhandari, S.V., and Kendre, M.V., 2024, Development of potential antidiabetic agents using 2D and 3D QSAR, molecular docking and ADME properties *in-silico* studies of α-amylase inhibitors, *Lett. Drug Des. Discovery*, 21 (16), 3443–3464.

[31] Sahoo, J., and Paidesetty, S.K., 2017, Antimicrobial activity of novel synthesized coumarin based transitional metal complexes, *J. Taibah Univ. Med. Sci.*, 12 (2), 115–124.

[32] Pichandi, M., and Shanmugam, S., 2024, Synthesis, characterization of Schiff base metal complexes with 1,3-propanediamine as secondary chelates and their DNA binding, DNA cleavage, cytotoxicity, antioxidant and activities, *J. Mol. Struct.*, 1307, 137932.

[33] Završnik, D., Muratović, S., Makuc, D., Plavec, J., Cetina, M., Nagl, A., De Clercq, E., Balzarini, J., and Mintas, M., 2011, Benzylidene-bis-(4-hydroxycoumarin) and benzopyrano-coumarin derivatives: Synthesis, $^{1}H/^{13}C$-NMR conformational and X-ray crystal structure studies and *in vitro* antiviral activity evaluations, *Molecules*, 16 (7), 6023–6040.

[34] Roy, N., Dutta, A., Mondal, P., Paul, P.C., and Sanjoy Singh, T., 2017, Coumarin based fluorescent probe for colorimetric detection of Fe^{3+} and fluorescence turn on-off response of Zn^{2+} and Cu^{2+}, *J. Fluoresc.*, 27 (4), 1307–1321.

[35] Dhayalan, V., Manikandan, C., Sharma, D., Dandela, R., 2022, "Recent Methods for Synthesis of Coumarin Derivatives and Their New Applications" in *Strategies for the Synthesis of Heterocycles and Their Applications*, Eds. Kumari, P., and Patel, A.B., IntechOpen, London, UK.

[36] Sharma, T., Singh, D., Mahapatra, A., Mohapatra, P., Sahoo, S., and Sahoo, S.K., 2022, Advancements in clinical translation of flavonoid nanoparticles for cancer treatment, *OpenNano*, 8, 100074.

[37] Souhangir, M., Bidoki, S.M., and Gharanjig, K., 2022, Synthesis of a novel fluorescent reactive dye based on coumarin-benzimidazole for high visibility dyeing of cotton, *Prog. Color, Color. Coat.*, 15 (4), 327–340.

[38] Stefanou, V., Matiadis, D., Tsironis, D., Igglessi-Markopoulou, O., McKee, V., and Markopoulos, J., 2018, Synthesis and single crystal X-ray diffraction studies of coumarin-based Zn(II) and Mn(II) complexes, involving supramolecular interactions, *Polyhedron*, 141, 289–295.

[39] Sunitha, N., Raj, C.I.S., and Kumari, B.S., 2023, Synthesis, spectral studies, biological evaluation and molecular docking studies of metal complexes from coumarin derivative, *J. Mol. Struct.*, 1285, 135443.

[40] Wen, M., Li, G., Liu, H., Chen, J., An, T., and Yamashita, H., 2019, Metal–organic framework-based nanomaterials for adsorption and photocatalytic degradation of gaseous pollutants: Recent progress and challenges, *Environ. Sci.: Nano*, 6 (4), 1006–1025.

[41] Yousef, T., Abu El-Reash, G.M., Abu AL-Zahab, M., and Safaan, M.A.A., 2019, Physicochemical investigations, biological studies of the Cr(III), Mn(II), Fe(III), Co(II), Ni(II), Cu(II), Zn(II), Cd(II), Hg(II) and UO_2(VI) complexes of picolinic acid hydrazide derivative: A combined experimental and computational approach, *J. Mol. Struct.*, 1197, 564–575.

[42] Zhang, G., Zheng, H., Guo, M., Du, L., Liu, G., and Wang, P., 2016, Synthesis of polymeric fluorescent brightener based on coumarin and its performances on paper as light stabilizer, fluorescent brightener and surface sizing agent, *Appl. Surf. Sci.*, 367, 167–173.